# Time scales of the Greenland Freshwater Anomaly in the Subpolar North Atlantic

**D.S. Dukhovskoy[1], I. Yashayaev[2], E.P. Chassignet[1], P.G. Myers[3], G. Platov[4], A. Proshutinsky[5]**

[1]Center for Ocean-Atmospheric Prediction Studies, Florida State University, Tallahassee, FL, USA.

[2]Bedford Institute of Oceanography, Fisheries and Oceans, Dartmouth, Nova Scotia, Canada.

[3]Department of Earth and Atmospheric Sciences, University of Alberta, University of Alberta, Edmonton, AB T6G 2E3, Canada.

[4]Institute of Computational Mathematics and Mathematical Geophysics, Novosibirsk, Russia.

Corresponding author: Dmitry Dukhovskoy (ddukhovskoy@fsu.edu)

[5]Woods Hole Oceanographic Institution, Woods Hole, MA, USA

## Abstract

Despite the increase in Greenland freshwater discharge, the impact of the Greenland freshwater anomaly (GFWA) on the Subpolar North Atlantic (SPNA) has been debated. It is unclear how long the GFWA remains in the SPNA and over what time frame the SPNA adjusts to the growing Greenland freshwater discharge. This study provides estimates for the response time required for the SPNA to adjust for increasing GFWA and residence time of the GFWA in the region. Time-evolving content of the GFWA in the SPNA is approximated with a first-order dynamical system and the response time is derived for different freshwater input functions. The solutions demonstrate that accumulation of the GFWA in the SPNA depends on the input function, yet they provide similar response time (13–16 years). The relation between response and residence times is derived and further investigated in Lagrangian experiments. The experiments show the residence time increasing with depth from 2 to 11 years at 50 m and 450 m, respectively. The difference is related to different convergence of the large-scale circulation in the upper (above 100 m) and deeper layers (100-800 m). As opposed to the observed intense short-lived freshening events in the SPNA, the weaker but more sustained GFWA is mainly accumulated in the subsurface layers. Being strongly dispersed over the water column the latter has a relatively small impact on salinity. Nevertheless, the content of the GFWA in the SPNA continues to increase making it comparable to freshwater content of preceding freshening events.

## 1 Introduction

With an annual mean freshwater flux around 1000 km$^3$ yr$^{-1}$, the Greenland Ice Sheet is an important freshwater source for the Subpolar North Atlantic (SPNA, figure 1). Greenland freshwater discharge (GFWD) has been increasing since the early 1990s (Bamber et al., 2012; 2018) (figures 2a and 2b). Integrated over the time period from 1993 to 2016, surplus GFWD from the Greenland Ice Sheet resulted in 5007 ± 390 km$^3$ of freshwater anomaly (Greenland freshwater anomaly, GFWA, figure 2c). Greenland freshwater is fluxed into the SPNA as direct freshwater (FW) flux from Greenland and with the ocean boundary currents from Baffin Bay and the northeast Greenland shelf. In situ observations provide evidence of Greenland FW presence in the SPNA. For example, analysis of measured noble gas distribution – often used to trace glacially modified water in high latitudes (Niu et al., 2015) – indicates a wide and deep spread of Greenland meltwater in the Labrador and Irminger Seas (Rhein et al., 2018). However, no certain quantitative estimates of the amount of the GFWA in the region can be easily derived from observations. Current estimates are mainly deduced from the model experiments with passive tracers that track the propagation of Greenland FW and show that most of this FW (up to 80%) is fluxed into the SPNA (Böning et al., 2016; Gillard et al., 2016; Luo et al., 2016; Dukhovskoy et al., 2016; 2019).

Therefore, the SPNA has experienced a substantial increase of surplus FW influx due to the accelerating GFWD over the last three decades. Many studies suggest that the volume of the GFWA accumulated in the SPNA is large enough to cause notable salinity shifts and impact convective processes in the region (Fichefet et al., 2003; Stouffer et al., 2006; Proshutinsky et al., 2015; Rahmstorf et al., 2015; Yang et al., 2016; Thornalley et al., 2018) but the question as to whether the GFWA truly impacts the SPNA remains unanswered (Böning et al., 2016; Frajka-Williams et al., 2016; Saenko et al., 2017). Several studies discuss the potential sources for the strong freshening that developed in the SPNA during the 2010s (Tesdal et al., 2018; Dukhovskoy et al., 2019; Holliday et al., 2020) including net precipitation and FW outflow from the Arctic Ocean in addition to the increased GFWD. The volume of the freshwater content anomaly in the SPNA accumulated during 2012–2016 is 6600 km$^3$ (Holliday et al., 2020) is comparable to the GFWA (5007 km$^3$ in 2016), but it is unclear if the two are related (Dukhovskoy et al., 2019). The uncertainty is mainly due to our lack of knowledge about accumulation time scales and rates of the GFWA in the SPNA.

The following questions motivate this study. How long does GFWA stay in the SPNA? How fast does the GFWA accumulate in the region and has it reached the maximal content? What salinity changes in the SPNA are caused by the GFWA? Can the GFWA cause freshening events similar to those previously observed in the SPNA? What fraction of the recently observed FW anomaly in the SPNA can be attributed to the surplus GFWD? The present study investigates the time scale over which the SPNA responds to the GFWA and residence time of the GFWA in the SPNA.

Given a relatively steady Greenland freshwater discharge before the 1990s (Bamber et al., 2018), an equilibrium between the inflow, outflow and volume (concentration) of Greenland freshwater in the SPNA can be assumed for that time frame. After the increase of the Greenland freshwater flux into the SPNA, the equilibrium was disturbed. The time over which the system adjusts to the changing FW influx and approaches a new equilibrium between the inflow, outflow and accumulated GFWA is characterized by the response time scale (more detail in section 2, see also Rodhe, 1992). We find that the time scale of the system response to the increased GFWD is inherently related to the residence time of the GFWA in the region (section 4).

The study region (SPNA, figure 1) comprises the Labrador Sea, the Irminger Sea and the central and eastern North Atlantic basins dynamically linked by a large-scale cyclonic circulation formed by the North Atlantic Current, Irminger Current, and the Labrador Current (Zhu and Demirov, 2011). The exchange between the SPNA and the adjacent northern basins is constricted by sills (shallower than 1000 m), whereas it has a broad deep opening at the southern boundary allowing interaction with the southern North Atlantic. The response time scale of the SPNA to the GFWA is derived by employing a first-order dynamical system describing a process of freshwater accumulation and release in the domain (section 2). The GFWA residence time scales are derived from Lagrangian particle tracking (section 5) using velocity fields from numerical experiments. The results suggest different mechanisms driving accumulation of freshwater anomaly in the SPNA for the GFWA and freshening events observed in the region (section 6).

## 2 Definitions and methodology

### *2.1 Greenland Freshwater Anomaly*

Estimates of GFWD are derived from a gridded product of Bamber et al. (2018). Annual GFWD can be expressed as a sum of the mean discharge ($\bar{F}_G$) and its anomaly ($F'_G$) (Figures 2a and 2b)

$$F_G(t) = \bar{F}_G + F'_G \tag{1}$$

The mean GFWD over 1958–1992 is 818.3 km$^3$ yr$^{-1}$. Average increase of GFWD during 1993–2016 is 209 ± 30 km$^3$ yr$^{-1}$. The GFWD anomaly is not constant but is increasing during this time period (Figure 2b) that can be approximated by a linear trend

$$F'_G(t) \approx \hat{F}'_G(t) = F_0 + p \cdot t \tag{2}$$

where $F_0$ = 21.8 km$^3$·yr$^{-1}$ and $p$ = 15.9 km$^3$·yr$^{-2}$.

The GFWA is defined as time-integrated GFWD anomaly from time $t_0$ to $t$ (Figure 2c)

$$V_{\mathrm{GFWA}}(t) = \int_{t0}^{t} F'_G(\tilde{t})\, d\tilde{t}. \tag{3}$$

In this study, the GFWA combines all components of the Greenland freshwater flux (Figure 2c). However, the increase in glacier meltwater discharge has dominated the contributions from the solid and tundra runoff discharges since 1994 (~65% since 2000, Figure 2c; 84% since 2009 in Enderlin et al., 2014). Integrated over the time period 1993–2016, the GFWA is 5007 ± 390 km$^3$.

### *2.2 Numerical experiments with Greenland passive tracers*

This study utilizes results from numerical experiments conducted within the Forum for Arctic Modeling and Observational Synthesis project (Proshutinsky et al., 2016). The analysis is primarily based on tracer experiments performed with a coupled 0.08º Arctic Ocean HYbrid Coordinate Ocean Model (HYCOM) (Bleck, 2002; Chassignet et al., 2006) and Los Alamos National Laboratory Sea Ice CodE (CICE) (Hunke and Lipscomb, 2008) (hereinafter referenced as HYCOM) configured for the North Atlantic, North Pacific and Arctic oceans and described in Dukhovskoy et al. (2019; hereinafter, D2019). The HYCOM has spatial resolution ~4.5 km in the study region. Results from similar tracer experiments performed with the 0.25º NEMO-LIM2 (Dukhovskoy et al., 2016; Gillard et al., 2016) and 0.25º SibCIOM (Golubeva and Platov, 2009; Dukhovskoy et al., 2016) were also used to discuss the oceanic GFWA fluxes into the SPNA.  In these numerical experiments, the propagation and accumulation of the GFWA was tracked by a passive tracer that was continuously released along the coast of Greenland at the freshwater sources. Locations and discharge rates of the Greenland freshwater sources were derived from a gridded product of Bamber et al. (2018). The flux of the passive tracer to the ocean was set proportional to the monthly Greenland freshwater discharge. Note that tracer concentration can be easily scaled to the GFWD anomaly (Appendix A, D2019). Tracer concentration in the domain was converted into the volume of GFWA at every grid cell of the model computational domain (see D2019 for detail). Shown in figure 2d are the HYCOM-based estimates of the GFWA accumulated in the SPNA for two scenarios of the GFWD anomaly: obtained from the dataset of Bamber et al. (2018) ($\tilde{V}_{GR}$) and the anomaly that was turned on in 1993 and kept constant at the average rate of 209 km$^3$ yr$^{-1}$ (step-function forcing, $\tilde{V}_{ST}$). By the end of 2016, 2240 km$^3$ of the GFWA were accumulated in the SPNA for realistic forcing and 2075 km$^3$ for the step-function forcing. These estimates will be used in the following analysis for the derivation of the time scales.

### *2.3 Fluxes of the Greenland Freshwater Anomaly into the SPNA*

There is direct influx of the GFWA into the SPNA from the southern sector of Greenland and indirect influx with the ocean boundary currents (figure 1). The direct flux of the GFWA into the SPNA averaged over 1993–2016 is around 70 km$^3$ yr$^{-1}$. Previous studies (Bönning et al., 2016; Dukhovskoy et al., 2016; D2019) suggest that substantial part of GFWD into other basins is fluxed into the SPNA within a relatively short period of time (within 1–2 years) especially on the eastern shelf where Greenland FW is transported by the East Greenland and East Greenland Coastal Currents. In the present study, simulated tracer and velocity fields from the model experiments were used to estimate transports of the GFWA into the SPNA through Denmark and Davis straits (figure 1) – the main routes of the GFWA into the region.

HYCOM-derived estimates of the oceanic fluxes of the GFWA through the straits agree with the estimates from NEMO (43 $km^3$ $yr^{-1}$ in Davis Strait and 50 $km^3$ $yr^{-1}$ in Denmark Strait) and SibCIOM (44 $km^3$ $yr^{-1}$ in Davis Strait and 51 $km^3$ $yr^{-1}$ in Denmark Strait). Most importantly, the total transport of the GFWA into the SPNA, which will be used in the following analysis, is similar across the simulations (93 – 97 $km^3$ $yr^{-1}$). Thus, combined direct and indirect fluxes of the GFWA into the SPNA is 167 $km^3$ $yr^{-1}$ ($\sim 0.8 \cdot F'_G$). Estimates of the total GFWA fluxes to the SPNA from NEMO and SibCIOM are similar to the HYCOM-based values (165 and 163 $km^3$, respectively).

*2.4 Dynamical System*

An analytical approach is designed to describe the accumulation of the GFWA in the SPNA resulting from the increased GFWD in order to estimate a time scale required for the analyzed system to adjust to the perturbed FW flux. In an idealized case with a step increase of the FW flux, a response time ($\tau$) characterizes a time scale for the system to reach a new equilibrium (steady state) after changed inflow (or outflow) rate. A new equilibrium would be characterized by changes in the mass (or concentration) of FW anomaly accumulated in the domain.

The following first-order autonomous dynamical system can be used to describe time-evolving changes in the system caused by a change in external conditions (e.g., Skogestad, 2009; Teschl, 2012)

$$\frac{dV(t)}{dt} + kV(t) - F(t) = 0, \tag{4}$$

$$V(t_0) = V_0, \tag{5}$$

where $F(t)$ is a forcing function describing external conditions (FW influx), $V(t)$ is dependent variable (volume of FW anomaly in the system), and $k = \tau^{-1}$ where $\tau$ is the system time constant (response time scale) that needs to be estimated for the SPNA. In general, $\tau$ determines how fast the system adjusts to the change in the forcing function. For the steady forcing conditions, $\tau$ provides a time scale required for the system state to change from $V_0(t_0)$ to $V(\infty)$ when the system approaches a new steady state (see section 4).

The model (4) with initial condition (5) describes the change in FW content of the SPNA caused by accumulated GFWA. An idealized case with no other salt fluxes but GFWA is considered, i.e. $V(t)$ is defined as

$$V(t) = \oiiint \frac{S_0(\mathbf{x},t) - S(\mathbf{x},t)}{S_0(\mathbf{x},t)} d\Omega, \tag{6}$$

where $S_0(\mathbf{x}, t)$ is the initial salinity field not impacted by the GFWA. Thus, $V(t)$ is the volume of the GFWA accumulated in the domain $\Omega$. The analytical solution of (4) can be compared with the estimate ($\tilde{V}$) derived from the tracer numerical experiments (figure 2d).

Changes in $V(t)$ are driven by $F(t)$, the influx of the GFWA into the system determined by the Greenland freshwater discharge anomaly (figure 2b). According to section 2.3, $F(t) = \alpha F'_G(t)$ and α=0.8. The second term ($kV$) describes export of the GFWA out of the SPNA.

## 3 Results

The general solution of (4) with the initial condition (5) is determined by the forcing function $F(t)$. Three cases are considered here: (1) $F(t)$ is a step function; (2) $F(t)$ is a linearly increasing function given by equation (2); (3) $F(t)$ is a bump function. The first two forcing functions approximate the fraction of the surplus GFWD fluxed into the SPNA. The third forcing function approximates an abrupt but short-period increase of FW flux (a pulse that is finite in time) into the SPNA. The step-function forcing approximates the surplus Greenland FW flux as an abrupt increase of the Greenland FW flux that is kept constant after 1993 at the value of the 1993-2016 mean flux anomaly fluxed into the SPNA. In the second case, the system is forced with a linearly increasing GFWA fluxed into the SPNA. The third case is designed to investigate the response of the system to a short-lived pulse of FW (of any origin) that are believed to cause wide-spread quickly developing freshening events in the SPNA similar to the GSA (e.g., Curry and Mauritzen, 2005).

### *3.1 Solution for a constant discharge anomaly*

The GFWD anomaly is a constant function $\Phi = \alpha F'_G$ imposed as a step function

$$F(t) = \Phi \cdot \mathrm{u}(t - t_0), \text{ where } \mathrm{u}(t - t_0) = \begin{cases} 1, & t \geq t_0 \\ 0, & t < t_0 \end{cases}, \qquad (7)$$

For this $F(t)$ and taking $t_0$=0, the solution that satisfies initial condition (5) is

$$V(t) = V_0 e^{-kt} + \frac{\Phi}{k}(1 - e^{-kt}) \qquad (8)$$

where $\Phi$ = 167 km$^3$·yr$^{-1}$ (section 2.2). Under a constant $F(t)$, the volume of the GFWA within the study region grows initially and then approaches a steady-state value (Figure 3a). Parameter $kt$ in the solution (8) is a dimensionless quantity and $(1 - e^{-kt})$ describes how fast the system approaches the new steady state ($V(\infty)$). Coefficient $k$ determines the value of the new steady state, i.e. it defines the volume of the GFWA accumulated in the SPNA when the system is adjusted to the increased FW flux.

To determine $k$, the solutions $V(t)$ are compared to the estimated $\tilde{V}_{ST}(t)$ derived from the HYCOM tracer experiments with constant GFWD anomaly (orange line in figure 2d). Based on the tracer budget, $\tilde{V}_{ST}(2016)$ is 2075 km$^3$. Taking $V_0$=0, equation (8) is solved iteratively yielding $k \approx 1/16$ suggesting that the response time scale $\tau$ is about 16 years (figure 3a).

### *3.2 Solution for a linearly increasing discharge anomaly*

The surplus Greenland freshwater discharge is not constant but has been accelerating at a nearly constant rate during 1993–2016 (Bamber et al., 2012; 2018). Therefore, a more realistic solution is obtained by using a linearly increasing discharge rate, which provides a reasonable approximation of the GFWD anomaly during this time period (figure 2b). The general solution of (4) with $F(t) = \hat{F}'_G(t)$ given by (equation 2) and with the initial condition (equation 5) is

$$V(t) = \frac{F_0}{k} + \frac{p}{k^2}(kt - 1) + \left(V_0 + \frac{p}{k^2} - \frac{F_0}{k}\right) e^{-kt}. \qquad (9)$$

The solution (equation 9) shows that the GFWA volume accumulated in the SPNA does not reach a steady state but continues to grow driven by the linearly increasing GFWD. This time,

$\tilde{V}_{GR}(t)$= 2240 km$^3$ is used to derive $k$. Eq. (9) is solved iteratively for $k$. The derived estimate is $k \approx 1/13$ yr$^{-1}$ and the time scale $\tau$ is about 13 years (figure 3b).

### *3.3 Solution for a bump forcing*

The GSA and freshening events of the 1980s and 1990s observed in the SPNA were attributed to pulses of excess FW released from the Arctic Ocean (Hakkinen, 1993; Belkin, 2004; Karcher et al., 2005). This is quite different from the GFWA that slowly evolves over several decades. The response of the SPNA to an abrupt pulse of FW can be predicted using the same system (eq. 4). In this case, the forcing function is represented as a bump function

$$F(t) = \Phi \cdot [\mathrm{u}(\mathrm{t} - a) - \mathrm{u}(\mathrm{t} - b)] \tag{10}$$

Where $t$=$a$ is time when the forcing is abruptly turned on and $t$=$b$ is time when the forcing is turned off. Using Laplace transform of (4) and (10) and taking $V_0$=0, solution for (4) with the forcing function (10) is found as

$$V(t) = \frac{\Phi}{k}\left\{u(t-a)\left[1 - e^{-k(t-a)}\right] - u(t-b)\left[1 - e^{-k(t-b)}\right]\right\}. \tag{11}$$

The width of the bump ($\Delta t = b - a$) represents the duration of the FW pulse. In the limit ($\Delta t \to 0$), the forcing becomes a delta function. The duration and the magnitude of the liquid FW pulse resulted in the GSA are 5 years and 2000 km$^3$·yr$^{-1}$, respectively following Curry and Mauritzen (2005). In this case, the solution demonstrates a different response of the system (figure 3c). The SPNA rapidly accumulates FW anomaly during the period of the increased FW flux and then, after the forcing is relaxed, FW anomaly slowly decays in the domain.

*3.4 Physical interpretation of the analytical solutions*

Three forcing functions representing different scenarios of FW influx into the SPNA result in different responses of the system (figure 3). The solution for the step function forcing (figure 3a) reaches a steady state quickly approaching the new steady state value $V(\infty)$ for time $t >> \tau$. When $t = 2\tau$, $V(\tau)$ is $0.87 \cdot V(\infty)$ (equation 9). Note that $V(t)$ cannot exceed $V(\infty)$ that is a function of $\tau$. For $\tau = 16$ years, $V(\infty)$ is 2670 $km^3$, which is substantially less than the volume of the FW anomaly during the GSA (10,000 $km^3$) or the 2010s freshening (6600 $km^3$). When the system reaches the new steady state, the outflow $kV$ equals the FW inflow, i.e., the system has adjusted to the new forcing reaching the balance between the inflow, outflow and the volume of the GFWA accumulated in the region.

The problem using a more realistic linearly increasing discharge anomaly ($\hat{F}'_G$) yields a solution that does not reach a steady state due to a linearly increasing FW flux rate (figure 3b). In the solution (eq. 9), the second term is negative for $t < \tau$ counteracting the exponential growth of the 3rd term. When $t > \tau$, the 2nd and 3rd terms are positive, however the contribution of the exponential term rapidly decays. Hence for this case, $\tau$ is the time scale indicating transition from a slow accumulation of the GFWA to a faster predominantly linear accumulation rate of the GFWA in the SPNA. Again, the volume of the GFWA accumulated in the SPNA by the end of 2016 is less than the volume of FW anomalies during the freshening events.

Therefore, the first two forcing functions representing an increase of GFWD result in different responses of the SPNA. However, the estimates of the response time scale ($\tau$) are similar (16 and 13 years). Note that in both cases, the shapes of the analytical solutions match remarkably well the GFWA volume in the SPNA derived from HYCOM (figures 2a and 2d) providing credibility to the analytical model describing accumulation of the GFWA in the SPNA.

The solution of the problem with the bump forcing function is expected to be qualitatively different from the two other solutions (figure 3c). After the forcing $F(t)$ is turned off ($t \geq t_b$), equation (4) describes the rate of removal of FWanomaly from the system. Thus, $k$ is sometimes referred to as the rate coefficient for removal (Schwartz, 1979). In this case, the response time scale can be interpreted as the time that it takes to reduce the volume of the accumulated water mass to $e^{-1}$ of its maximum at $t_b$ (e-folding time). Also $\tau$ determines the peak value of the FW anomaly in the SPNA. For considered cases, the analytical solutions predict the maximum volume of the FW anomaly during the GSA in the range from ~6000 to 9800 $km^3$ for different $k$.

## 4. Relation between response and residence time scales

Analytical solutions of the dynamical system (4) describing accumulation of the GFWA in the SPNA provide time estimates of the system response (or adjustment) to different regimes of GFWA introduced into the system. However, observational-based studies characterize time scales of FW anomalies in the SPNA in terms of residence time including transit time (e.g., Belkin, 2004; Yashayaev et al., 2015). Are these two time scales related? The residence time ($\tau_r$) of a water mass or a set of water parcels in a control volume Ω can be defined in terms of three time quantities (Bolin & Rodhe, 1973): Turn-over time ($\tau_{to}$), mean age ($\tau_{ma}$), and mean transit ($\tau_{mt}$) time. Turn-over time is the ratio of the volume of the water mass (here, GFWA) to the inflow rate or outflow rate. Mean age is the average age of parcels in Ω. Mean transit time is the average age of water parcels leaving Ω.

Thus, a relationship between the response time scale $\tau$ and residence time ($\tau_r$) of the GFWA in the SPNA is sought. The two terms are related but not necessarily identical, especially for a non-steady case. For a residence time approaching zero, the GFWA would not accumulate in the region and the response time scale would be approaching 0 as well. Conversly, for an infinitely long residence time, the total volume of the GFWA fluxed into the SPNA would remain in the domain and response time scale would be infinitely large.

### *4.1. Constant discharge anomaly*

A system forced with a constant discharge anomaly after an abrupt increase (step function) results in a steady-state solution. Relating the response time scale $\tau$ with the residence time for a steady case is straight forward. For processes that can be described as the first order dynamical system (equation 4) $\tau$ may be interpreted as any of the time quantities because all the above residence times are equal to the $k^{-1}$ (Schwartz, 1979). Note that under the steady state, the turn-over time and the mean transit time are equal (Bolin & Rodhe, 1973), thus the turn-over time can be derived from either inflow or outflow rates given the volume of the water mass in the domain. For example, the turn-over time ($\tau_{to}$) of the GFWA can be easily derived from (equation 4) under the steady-state condition

$$\tau_{to} = \frac{V(\infty)}{\Phi}. \qquad (12)$$

Noting that $V(\tau)$=0.63$V(\infty)$ (section 3.3) and $V(\tau)$=1683 km$^3$ (figure 3a), $\tau_{to}$ is 16 years, which equals $\tau$ derived from the analytical solution by iteration.

### *4.2. Linearly increasing discharge anomaly*

For the linearly increasing discharge anomaly, the relationship between $\tau$ and $\tau_r$ is more complex because the solution is non-steady-state. The following relations are derived for the study case based on Schwartz (1979). The turn-over time is not uniquely defined because the inflow and outflow of the GFWA are not equal for a non-steady-state case. Hence, there are two possible definitions of $\tau_{to}$ (eqs. 13 and 14) relating the amount of water mass present in Ω at time $t$ to the inflow and outflow rates, respectively.

$$\tau_{to}^{(1)} = \frac{V(t)}{F(t)}, \qquad (13)$$

$$\tau_{to}^{(2)} = \frac{V(t)}{kV(t)} = k^{-1} = \tau. \qquad (14)$$

Note that the time scales are time-dependent and, in general, the two definitions of the turn-over time are not identical. The second definition equals the response time scale from the analytical solution. The turn-over time scale $\tau_{to}^{(1)}$ is shown in figure (4) for $k$ = 1/13 (derived for the GFWA in section 3.2). The time scale converges to $k^{-1}$=13 years, which is $\tau_{to}^{(2)}$ and the response time scale. Therefore, for the analyzed system, the response time scale derived from the analytical model (eq. 4) provides an estimate for the turn-over time of the GFWA fluxed into the SPNA at a linearly increasing rate.

For the analyzed dynamical system (eq. 4), the mean transit time is equal to the mean age (Schwarts, 1973), meaning that the average time GFWA spends in the SPNA equals the mean transit time for the GFWA. The mean transit time for the non-steady solution is

$$\tau_{mt}(t) = \frac{1}{V(t)} \int_0^t (t - t_0) F(t_0) e^{-k(t-t_0)} dt_0, \qquad (15)$$

where $F(t) = \hat{F}'_G(t)$ is the linearly-increasing forcing function (2). The mean transit time also converges to $k^{-1}$=13 years as $t \to \infty$ (figure 4). Hence, the analytically derived response time scale provides an estimate for the limits of the transit time and mean age of the GFWA for the non-steady state solution as $t \to \infty$.

## 5. Residence time scale from Lagrangian analysis

### *5.1. Experiments with Lagrangian particles*

In addition to the analytical estimates of the time scales presented in the previous sections, we now evaluate the time scales by performing Lagrangian experiments in HYCOM. Lagrangian modelling has been widely used for the derivation of residence time scales and pathways of water masses in the ocean (e.g., van Sebille et al., 2018). In this study, GFWA is discretized with 1800 Lagrangian particles that are randomly seeded on the southwestern shelf (the blue shaded area in figure 1) and advected by the high-resolution (~4.5 km) daily mean HYCOM velocity fields using explicit 4-stage Runge-Kutta method with a two-day time stepping. The release location is chosen based on D2019 who showed that >80% of the Greenland freshwater outflow takes places on the southwestern shelf (see also Schulze Chretien and Frajka-Williams, 2018). The experiment was performed for the time period from 1993 through the end of 2019.

The importance of subsurface export of Greenland meltwater has been discussed in previous studies (Straneo et al., 2011; Beaird et al., 2015). Analysis of noble gases tracing glacial meltwater indicated deep spreading of Greenland FW in the North Atlantic (Rhein et al., 2018). Similar results were presented by D2019 who showed that GFWA is quickly mixed downward on the southeastern Greenland shelf due to persistent downwelling winds, in agreement with other studies (e.g., Sutherland and Pickart, 2008). In order to track propagation of the GFWA at different depths, the particles are released at one time in 4 model layers nominally representing depths of 50 m (group 1), 90 m (group 2), 150 m (group 3), and 450 m (group 4) in the deep ocean. Each group has 600 particles. Note that HYCOM hybrid vertical layers follow isopycnals in the deep ocean and become terrain-following layers on the shelf. When interpreting the results, it should be kept in mind that in HYCOM isopycnal layers the particles are advected along the isopycnal surfaces (similar to a real-life advection of water masses, see Bleck, 1998; 2002) whose depth varies in time and space. Over the shelf, HYCOM layers become terrain-following and the thicknesses (and depths) of all layers are adjusted accordingly. Thus, over the shelf region the release depths of the particles can be shallower than the nominal depths.

The Lagrangian experiments are used to quantify a residence time scale of the GFWA in terms of transit time, which equals the age of the particles in this experiment. The age of ocean water masses can be presented in terms of the transit time distribution (van Sebille et al., 2018). The transit time is the difference between the time when the particle leaves the domain and the release time. In this analysis, the particle is considered to leave the domain if it has stayed out of the domain longer than 90 days to allow for recirculation of the GFWA with mesoscale eddies.

### *5.2. Results of the Lagrangian experiments*

The Lagrangian particles from all 4 groups leave the western shelf and circulate cyclonically over the northern and western Labrador Sea with the Labrador Current during the 1st year (figure 5). During this time, only a small number of particles have travelled to Baffin Bay, most likely due to the release time, January, when the shelf northward flow is weak (Luo et al., 2016). The particles from group 4 (450 m) stay along the continental shelf slope when travelling around the northern and western Labrador Sea, whereas the particles from the other groups stay more onshore. After the first year, the particles in the first three groups reach the southern boundary of the SPNA where they become entrained into the northward flowing jets of the North Atlantic current. Most of the particles from the 4$^{th}$ group make a northward turn into the Irminger Sea (see animation in Supplemental Material). After the 1$^{st}$ year, the particles from all groups circulate in the SPNA, leaving the domain as time progresses. There is a remarkable difference in the rate at which the particles from different groups leave the domain. Most of the particles advected in the upper 50 m leave the SPNA during the first 10 years, whereas the particles from the other groups leave the domain at a notably slower rate, especially those advected at 450 m.

The pathways of the particles are deduced from probability maps (figure 6) derived from the counts of particles in the grid cells and normalized by the total number of counts. The probability maps show that the particles circulate in the SPNA, staying predominantly in the

Labrador, Irminger and central North Atlantic. There is, however, a notable difference in the circulation patterns among the particles from different groups. Except for the release location on the southwestern Greenland shelf, the occurrence probability of the particles from groups 2, 3, and 4 on the shelves is low indicating that the particles in the subsurface layers tend to circulate in the deep SPNA. Particles in the surface layer (group 1) have more frequent presence on the shelves especially near Newfoundland (figure 6a). The particles form all groups have a high occurrence probability in the deep southwestern Labarador Sea, whereas the pathways of the particles in the central and eastern interior SPNA depend on the particles' depth. The particles advected at 150 m and 450 m have the highest occurrence probability in these areas.

A different exchange pattern between the SPNA and adjacent basins is demonstrated by the particles' pathways (also evident in figure 5). For group 4, the northward exchange of the particles is limited to Baffin Bay with nearly absent transport to the Nordic Seas. This suggests that the GFWA spreads into Baffin Bay from the SPNA along the isopycnals, forming subsurface freshening in the central basin below the maximum depth of winter convection (Tang et al., 2004). Similar results were discussed in (Dukhovskoy et al., 2016; D2019). The northward transport of particles at shallower isopycnal layers is predominantly into the Nordic Seas, although the transport to Baffin Bay over the Greenland shelf is notable as well.

Derived distributions of the age and transit time (figures 7 and 8) of the particles provide estimates for the residence time scales of the GFWA in the SPNA. For these experiments, the age and transit time distributions are similar, in agreement with the earlier discussion in section 4.2. The main finding from the distributions is that the residence time depends on the depth of the layers where the particles have been advected. The particles advected in the near-surface layer (50 m) tend to leave the SPNA during the first 1–3 years (figure 7a). The probability that the age or transit time of the particles from group 1 exceeds N years quickly decays as N increase (bars in figure 8a). Alternatively, the probability that the age or transit time is less than or equal to N years quickly increases for $N<10$ (black line in figure 8a). The distributions for groups 3 and 4 are flatter (figures 7c and d), indicating that the particles in the deeper layers stay markedly longer in the SPNA. The result is more evident in the diagram presenting the median of the age / transit time with the interdecile ranges (figure 8e). There is an obvious increase of the particles' age and transit time (hence, residence time) in the SPNA with depth.

Therefore, the Lagrangian experiments provide the following estimates of the GFWA residence time in the SPNA. In the near-surface layer (50 m), the median residence time is 2–3 years (the interdecile range is 1–9 years). At 90 m nominal depth, the median residence time is 7 years (2–16 years). At 150 m, the median residence time is 9 years (2–22 years). At 450 m, the median residence time is 11 years (3–27 years).

## 6. Discussion

### *6.1. SPNA response to the GFWA and freshwater pulses*

Analytical solutions of the first-order autonomous dynamical system (eq. 4) used to describe time evolution of FW anomaly in the SPNA were derived for different forcing functions approximating three scenarios of changes in the FW flux into the domain: a step-function, an increasing linear trend, and a bump function.  The solutions demonstrate qualitatively different responses of the dynamic system to the three forcing functions suggesting different evolution of

FW anomaly in the SPNA for these three cases (figure 3). For the linearly increasing case, the system does not reach a steady state. Instead, GFWA accumulated in the SPNA grows almost linearly after the response time scale $\tau$.

A slowdown of the freshwater discharge anomaly from the Greenland Ice Sheet occurred during 2012–2016 (figure 2b). If the hiatus continues long enough ($t \gg \tau$) and the surplus discharge rate remains at ~300 $km^3\ yr^{-1}$ (the rate during 2012–2016, figure 2b), a new steady state value of the GFWA content that will be reached by the SPNA is ~4800 $km^3$ (eq. 8). Recent satellite data revealed an unprecedented summer mass loss of the Greenland Ice Sheet in 2019 (Velicogna et al., 2020), which may indicate the return of an accelerating GFWD.

Solutions obtained for the linearly increasing FW flux predicts a slower accumulation rate of FW anomaly in the domain during the first several years after the forcing is turned on (i.e. after 1993 in figure 3) compared to the other two cases. This is particularly important when comparing responses to the GFWA and to pulses of FW periodically observed in the Fram Strait (de Steur et al., 2018) that potentially result in the development of freshening events in the SPNA. According to the analytical solution (eq. 11), after the pulse of FW has reached the SPNA, FW anomaly quickly accumulates within the domain. After the pulse has passed, FW anomaly leaves the SPNA at a rate determined by the residence time scale (figure 3c). Hence, the accumulation rate of FW anomaly in the SPNA would be slower for the GFWA than for a FW pulse.

*5.2. Why does the residence time increase with depth?*

The next important finding of this study is depth-dependence of the residence time scale of the GFWA demonstrated in the experiments with Lagrangian particles (figure 7 and 8). The experiments indicate that the median residence time of the GFWA in the upper 50 m is only 3 years, which is markedly smaller than the analytically derived response time scale (13 years). In the deep subsurface layers (below 150 m), the median residence time is 11 years that is close (compared to the broad interdecile ranges for these groups) to the response time scale. The results imply that accumulation of the GFWA mainly occurs in the subsurface layers (below 100 m), whereas FW anomalies in the upper ocean are transient and leave the domain within 2–3 years.

A possible explanation of the depth dependency of the GFWA residence time could be merely due to slower ocean circulation in the subsurface layers compared to the upper ocean largely wind-driven flows. However, we speculate that the depth dependency might also be a manifestation of different large-scale circulation in the SPNA in the upper ocean and subsurface layers. The large-scale cyclonic circulation of the upper ocean in the SPNA is divergent meaning that the long-term mean transport of water masses is out of the domain. This explains the short residence time of the Lagrangian particles in the simulations. We suggest that the subsurface (below ~100 m) large-scale circulation in the SPNA is convergent.

In order to test this assertion, we employ the Gauss theorem to calculate the normal flux across the contour $\Gamma$ bounding the SPNA (figure 1) to derive the divergence of the flow inside the domain $\Omega$

$$\iiint_{\Omega} \nabla_h \cdot \vec{U} d\Omega = \oiint_{\partial\Gamma} \vec{U} \cdot \vec{n}\, d\Gamma \qquad (16)$$

where $\vec{n}$ is an outward normal unit vector. It can be shown that

$$\oiint_{\partial\Gamma} \vec{U} \cdot \vec{n}\, d\Gamma = \sum_{\partial\Gamma_i \subset \partial\Gamma} \oiint_{\partial\Gamma_i} \vec{U} \cdot \vec{n}\, d\Gamma_i = \sum_{\partial\Gamma_i \subset \partial\Gamma} M_i, \qquad (17)$$

where $\Gamma_i$ is surface bounding a subvolume $\Omega_i \subset \Omega$, i.e. the total flux through $\Gamma$ is calculated by layers to gain the volume-integrated divergence within the individual model layers. The volume flux through $\Gamma_i$ is $M_i$. Obviously, the total volume flux across the contour is $\sum_i M_i = 0$. Individual volume fluxes ($M_i$) provide information about divergence within the subvolume $\Omega_i$ (figure 9). Positive $M_i$ corresponds to water mass outflow and divergence in the subvolume (model layer). The daily mean velocity fields were derived from the HYCOM tracer experiment (D2019). The volume fluxes were averaged in time.

There is strong divergence in the upper ocean (~100 m) in the SPNA (figure 9). In the summer, the divergence in the upper ocean is stronger and shallower than in the winter. The upper ocean divergence is presumably associated with the large-scale cyclonic circulation in the SPNA. Lagrangian particles from group 1 were advected within the near-surface layer of strong divergence resulting in a short residence time of this group.

By contrast, strong and persistent convergence is observed in the layer between 100 and 800 m in figure 9. Physical processes driving convergence in this layer require further investigation beyond the scope of our study. However, we suggest that the convergence is driven by the inflow compensating for the mass loss within the upper divergent layer. Particles from groups 3 and 4 travelled within the convergent layer, thus they have longer residence time than particles from group 1. This result concurs with previous studies that reported the existence of recirculation cells in the subsurface layers of the SPNA where profiling floats were trapped during the observational experiments (Lavender et al., 2000; 2005; Fischer et al., 2018).

The analysis used HYCOM high-resolution 3D velocity fields. Such information is not readily available from observations, which limits the possibility to validate these results. Investigation of the large-scale circulation in the subsurface SPNA using data from the autonomous Lagrangian platforms (similar to Palter et al., 2016; Fischer et al., 2018; Bower et al., 2019) could be a research objective for a separate study.

### *6.3. GFWA and freshening events in the SPNA*

The above results suggest different evolutions of FW anomaly and associated freshening in the SPNA originated from the GFWA and FW pulses propagating from the Arctic Ocean (either through Fram Strait or Davis Strait). The GFWA is fluxed into the SPNA at a slow but continuous rate. This surplus FW does not impact the water column stability greatly and FW is mixed into the deeper layers by wind-driven mixing (especially on the Greenland shelf (Sutherland and Pickart, 2008; Luo et al., 2016; D2019)) and with the deep convection in the interior SPNA (Yashayaev and Loder, 2016; 2017). Therefore, a substantial fraction of the GFWA propagates into subsurface layers below 100 m where it circulates, trapped within the SPNA by the large-scale convergent flows. Whereas, in the near-surface layers (above 100 m), GFWA is quickly removed from the SPNA by the predominantly divergent large-scale circulation. Therefore, most of the GFWA accumulated in the SPNA is stored below 100 m, while surface salinity remains largely unaffected. The GFWA is dispersed over the water column due to intense vertical mixing. This is supported in a study by Rhein et al. (2018) who used noble gases to trace Greenland meltwater in the SPNA and found the presence of meltwater in the deep Labrador and Irminger Sea. Thus, the overall impact of the GFWA on salinity in the SPNA is expected to be small. This is in agreement with estimated salinity changes in the SPNA caused by the GFWA derived from the tracer experiments in D2019. The changes are in the order of 0.01. Therefore, the presence of the GFWA is not easily identified in salinity observations. Accurate calculation of the FW content change over the whole water column should provide evidence of the GFWA accumulation in the region.

In the cases of FW pulses, the flux of FW anomaly transported into the SPNA is about 10 times larger than the surplus Greenland FW flux. This leads to quick accumulation of FW anomaly in the SPNA (figure 3c). Due to the large volume quickly advected into the SPNA, the FW anomaly substantially shifts surface salinity and water column stability inhibiting its vertical mixing and spreading into the subsurface layers. Therefore, the FW anomaly predominantly stays in the near-surface layers causing strong freshening in the SPNA. The anomaly leaves the domain in less than 10 years as indicated by the residence time of the Lagrangian particles in the upper layers (figure 8e).

With regard to the 2010s freshening in the SPNA, the direct relation to the GFWA is unlikely. Observed freshening with magnitudes 0.1–0.3 developed quickly and primarily in the upper 200 m (D2019; Holliday et al., 2020), which is more characteristic of a FW pulse propagating into the SPNA (figure 3). However, the GFWA could have contributed to the overall FW content anomaly in the SPNA. According to Holliday et al. (2020), the upper 1000 m of the SPNA acquired about 6600 $km^3$ of FW anomaly during 2012–2016. Deep propagation and a wide spreading of the freshening in the SPNA could be attributed to the accumulated GFWA in the subsurface layers.

## 7. Conclusions

The results of our study are summarized here as answers to the questions formulated in section 1. First, experiments with Lagrangian particles have demonstrated markedly different residence times for the particles advected at different depths. The results suggest that residence time of the GFWA (or any other FW anomaly) in the top 50 m of the SPNA is 2 years and increases with depth reaching 11 years at 450 m. It has been suggested that the increase of the residence time with depth could be due to different convergence of the large-scale circulation in the upper ocean and subsurface (100–800 m) layers.

Second, the analytical solutions (figure 3) demonstrate that the system responds to the increased GFWD by growing content of the GFWA. Accumulation rate of the GFWA in the SPNA can be derived by differentiating the analytical solutions (equations 8–11). The solutions have demonstrated differences in time-evolving accumulation of FW anomaly in the SPNA for different FW forcing functions. Solution for the linearly increasing $F'_G(t)$ (eq. 2) does not reach a steady state, which means that accelerating Greenland melt results in a still growing volume of FW anomaly in the SPNA. Compared to the bump forcing case, the non-steady state solutions suggest a relatively slow accumulation rate of GFWA within the time scales of a FW pulse for similar response time scales.

Third, the GFWA is greatly dispersed in the water column and the overall impact of the GFWA on salinity in the SPNA is expected to be small. Estimated salinity changes in the SPNA caused by the GFWA by the end of 2016 is O(0.01) reported in D2019.

Fourth, derived estimates of the GFWA residence time and time-evolving content of the GFWA in the SPNA demonstrate slow accumulation of the FW anomaly in the subsurface layer (below 100 m) with a relatively small (compared to the previous freshening events) impact on salinity. This is different from observed freshening events in the SPNA that are characterized by quick (less than 5 years) development of strong negative salinity anomaly in the upper ocean propagating across the domain on a decadal time scale. Thus, we conclude that at present increase of GFWD the GFWA cannot cause freshening events similar to the observed events.

Fifth, estimated volume of the GFWA accumulated in the SPNA of 2240 $km^3$ has been used in this analysis (derived in D2019). This is roughly 30% of the estimated FW content anomaly during the 2010s freshening (Holliday et al., 2020). Nevertheless, the GFWA content in the SPNA continues to grow and in the future, may cause a substantial shift in salinity fields.

**Acknowledgments, Samples, and Data**


- The daily mean fields from the 0.08 AO HYCOM experiment with the passive tracer are available at the HYCOM data server (ftp://ftp.hycom.org/datasets/ARCc0.08/expt_11.0/data/).
- D.S. Dukhovskoy and E.P. Chassignet were funded by the DOE (award DE-SC0014378) and HYCOM NOPP (award N00014-19-1-2674). The HYCOM-CICE simulations were

supported by a grant of computer time from the DoD High-Performance Computing Modernization Program at NRL SSC.

- G. Platov was funded by the RSF N19-17-00154.
- P.G. Myers was funded by an NSERC Discovery Grant (Grant RGPIN 04357). The NEMO simulations were supported by Compute Canada (http://www.computecanada.ca)
- A. Proshutinsky was funded by FAMOS project (NSF grant # NSF 14-584)

**References**

Bamber, J., M. van den Broeke, J. Ettema, J. Lenaerts, and E. Rignot, 2012: Recent large increases in freshwater fluxes from Greenland into the North Atlantic, *Geophysical Research Letters*, **39**, L19501. https://doi.org/10.1029/2012GL052552.

Bamber, J. L., A. J. Tedstone, M. D. King, I. M. Howat, E. M. Enderlin, M. R. van den Broeke, and B. Noel, 2018: Land ice freshwater budget of the Arctic and North Atlantic Oceans 1. Data, methods, and results. *Journal of Geophysical Research: Oceans,* **123**, 1827–1837. https://doi.org/10.1002/2017JC013605.

Beaird, N., F. Straneo, and W. Jenkins, 2015: Spreading of Greenland meltwaters in the ocean revealed by noble gases, *Geophys.Res. Lett.*, **42**, 7705– 7713,doi:10.1002/2015GL065003

Belkin, I., 2004: Propagation of the “Great Salinity Anomaly” of the 1990s around the northern North Atlantic, *GRL*, **31**, L08306, doi:10.1029/2003GL019334.

Bleck, R., 1998: Ocean modeling in isopycnic coordinates. In: Chassignet, E.P., Verron, J. (Eds.), Ocean Modeling and Parameterization, NATO Science Series, *Kluwer Academic Publishers*, pp. 423-448.

Bleck, R., 2002: An oceanic general circulation model framed in hybrid isopycnic-Cartesian coordinates, *Ocean Modelling*, **37**, 55-88.

Bolin, B., and H. Rodhe, 1973: A note on the concepts of age distribution and transit time in natural reservoirs, *Tellus* **25**, 58-62.

Böning, C.W., M. Scheinert, J. Dengg, A. Biastoch, and A. Funk, 2016: Decadal variability of subpolar gyre transport and its reverberation in the North Atlantic overturning, *GRL*, **33**, L21S01, doi:10.1029/2006GL026906.

Bower, A., et al., 2019: Lagrangian views of the pathways of the Atlantic Meridional Overturning Circulation, *JGR-Oceans*, **124**, 5313–5335, https://doi.org/10.1029/2019JC015014 .

Chassignet, E. P., and Coauthors, 2006: Generalized vertical coordinates for eddy-resolving global and coastal ocean forecasts. *Oceanography*, **19**, 20–31.

Curry, R. and C. Mauritzen, 2005: Dilution of the Northern North Atlantic Ocean in recent decades, *Science*, **308**, 1772–1774.

De Steur, L., C. Peralta-Ferriz, and O. Pavlova, 2018: Freshwater export in the East Greenland Current freshens the North Atlantic. *Geophysical Research Letters*, **45**, 13, 359–13, 366. https://doi.org/10.1029/2018GL080207.

Dukhovskoy, D. S., and Coauthors, 2016: Greenland freshwater pathways in the sub-Arctic Seas from model experiments with passive tracers. *Journal of Geophysical Research: Oceans*, **121**, 877–907, https://doi. org/10.1002/2015JC011290.

Dukhovskoy, D. S., I. Yashayaev, A. Proshutinsky, J. L. Bamber, I. L. Bashmachnikov, E.P. Chassignet, C.M. Lee, and A.J. Tedstone, 2019: Role of Greenland freshwater anomaly in the recent freshening of the subpolar North Atlantic. *Journal of Geophysical Research: Oceans*, **124**. https://doi.org/ 10.1029/2018JC014686

Enderlin, E. M., I. M. Howat, S. Jeong, M.-J. Noh, J. H. van Angelen, and M. R. van den Broeke, 2014: An improved mass budget for the Greenland ice sheet, *Geophys. Res. Lett.*, **41**, 866–872, doi:10.1002/2013GL059010

Fichefet, T., C. Poncin, H. Goosse, P. Huybrechts, I. Janssens, and H. LeTreut, 2003: Implications of changes in freshwater flux from the Greenland Ice Sheet for the climate of the 21st century. *Geophysical Research Letters*, **30(17)**, 1911. https://doi.org/10.1029/2003GL017826

Fischer, J., J. Karstensen, M.Oltmanns, and S. Schmidtko, 2018: Mean circulation and EKE distribution in the Labrador Sea Water level of the subpolar North Atlantic, *Ocean Sci.*, **14**, 1167–1183.

Frajka-Williams, E., J.L. Bamber, and K. Våge, 2016: Greenland melt and the Atlantic meridional overturning circulation. *Oceanography,* **29**(4):22–33, https://doi.org/10.5670/oceanog.2016.96.

Gillard, L.C., X.Hu, P.G. Myers, and J. L. Bamber, 2016: Meltwater pathways from marine terminating glaciers of the Greenland ice sheet, *Geophys. Res. Lett.,* **43**, 10,873–10,882,doi:10.1002/2016GL070969

Golubeva, E.N., and G.A. Platov, 2009: Numerical modeling of the Arctic Ocean ice system response to variations in the atmospheric circulation from 1948 to 2007. *Izv. Atmos. Ocean. Phys.* **45**, 137–151, doi:10.1134/S0001433809010095.

Häkkinen, S., 1993: An Arctic source for the great salinity anomaly: A simulation of the Arctic ice-ocean system for 1955–1975, *JGR*, **98**(C9), 16397-16410.

Holliday, N. P. and Coauthors, 2008: Reversal of the 1960s to 1990s freshening trend in the northeast North Atlantic and Nordic Seas, *Geophys. Res. Lett.*, **35**, L03614.

Holliday, N.P., and Coauthors, 2020: Ocean circulation causes the largest freshening event for 120 years in eastern subpolar North Atlantic, *Nat Commun.*, **11**, 585, https://doi.org/10.1038/s41467-020-14474-y

Hunke, E. C., and W. Lipscomb, 2008: CICE: The Los Alamos Sea Ice Model: Documentation and Software User's Manual, Version 4.0, Tech. Rep. LA-CC-06-012, Los Alamos Natl. Lab., Los Alamos, NM.

Karcher, M., R. Gerdes, F. Kauker, C. Koberle, and I. Yashayaev, 2005: Arctic Ocean change heralds North Atlantic freshening, *Geophys. Res. Lett.*, **32**, L21606, doi:10.1029/2005GL023861.

Lavender, K. L., R.E. Davis, and W.B. Owens, 2000: Mid-depth recirculation observed in the interior Labrador and Irminger seas by direct velocity measurements, *Nature*, **407**, 66–69, 2000.

Lavender, K. L., W.B. Owens, and R.E. Davis, 2005: The mid-depth circulation of the subpolar North Atlantic Ocean as measured by subsurface floats, *Deep-Sea Res. I*, **52**, 767–785, https://doi.org/10.1016/j.dsr.2004.12.007,.

Luo, H., R. Castelao, A.K. Rennermalm, M. Tedesco, A. Bracco, P. L. Yager, and T. L. Mote, 2016: Oceanic transport of surface meltwater from the southern Greenland ice sheet. *Nature Geosci.,* **9**, 528–532, https://doi.org/10.1038/ngeo2708

Niu, Y., M. C. Castro, S. M. Aciego,C. M. Hall, E. I. Stevenson, C. A. Arendt, and S. B. Das 2015: Noble gas signatures in Greenland: Tracing glacial meltwater sources, *Geophys. Res. Lett.*, **42**, 9311–9318, doi:10.1002/2015GL065778.

Palter, J. B., C. A Caron, K. L. Law, J. K Willis, D. S. Trossman, I. M. Yashayaev, and D. Gilbert, 2016: Variability of the directly observed, mid depth subpolar North Atlantic circulation, *Geophys. Res. Lett.*, **42**, 2700–2708, https://doi.org/10.1002/2015GL067235.

Proshutinsky, A., D. Dukhovskoy, M.-L. Timmermans, R. Krishfield, and J. Bamber, 2015: Arctic circulation regimes. *Philosophical Transactions Royal Society A*, A, 373(2052), 20140160. https://doi.org/10.1098/rsta.2014.0160

Rahmstorf, S., J. E. Box, G. Feulner, M. E. Mann, A. Robinson, S. Rutherford, and E. J. Schaernicht, 2015: Exceptional twentieth-century slow-down in Atlantic Ocean overturning circulation. *Nature Climate Change*, 5, 475–480. https://doi.org/10.1038/nclimate2554

Rhein, M., R. Steinfeldt, O. Huhn, J. Sültenfuß, and T. Breckenfelder, 2018: Greenland submarine melt water observed in the Labrador and Irminger Sea. Geophysical Research Letters, 45, 10,570–10,578. https://doi.org/10.1029/2018GL079110

Rodhe, H., 1992: Modeling Biogeochemical Cycles, in Global Biogeochemical Cycles, Eds. S.S. Butcher et al., Academic Press, London, pp. 367, p. 55-72

Saenko, O. A., D. Yang, and P. G. Myers, 2017: Response of the North Atlantic dynamic sea level and circulation to Greenland meltwater and climate change in an eddy-permitting ocean model. *Climate Dynamics*, **49**, 2895–2910. https://doi.org/10.1007/s00382-016-3495-7

Schulze Chretien, L.M. and E. Frajka-Williams, 2018: Wind-driven transport of fresh shelf water into the upper 30 m of the Labrador Sea, *Ocean Sci.*, **14**, 1247–1264, 2018 https://doi.org/10.5194/os-14-1247-2018.

Schwartz, S.E., 1979: Residence times in reservoirs under non-steady-state conditions: application to atmospheric CO2 and aerosol sulfate, *Tellus*, **31**, 530-547.

Skogestad, S., 2009: Process Dynamics, in “Chemical and Energy Process Engineering”, *CRC Press Taylor & Francis Group*, LLC, USA, 440 pp.

Straneo, F., R. G. Curry, D. A. Sutherland, G. S. Hamilton, C. Cenedese, K. Våge, and L. A. Stearns, 2011: Impact of fjord dynamics and glacial runoff on the circulation near Helheim Glacier, *Nat. Geosci.*, **4**(5), 322–327, doi:10.1038/ngeo1109.

Stouffer, R. J., and Coauthors, 2006: Investigating the causes of the response of the thermohaline circulation to past and future climate changes. *Journal of Climate*, **19**(8), 1365–1387. https://doi.org/10.1175/JCLI3689.1

Sutherland, D. and R. Pickart, 2008: The East Greenland Coastal Current: Structure, variability and forcing, *Progr. Oceanogr.*, **78**, 58–77.

Tang, C. C. L., Ross, C. K., Yao, T., Petrie, B., DeTracey, B. M., & Dunlap, E., 2004: The circulation, water masses and sea-ice of Baffin Bay. *Progress in Oceanography,* **63(4)**, 183–228. https://doi.org/10.1016/j.pocean.2004.09.005

Teschl, G., 2012: Ordinary Differential Equations and Dynamical Systems, AMS, 356 pp.

Thornalley, D. J. R., and Coauthors, 2018: Anomalously weak Labrador Sea convection and Atlantic overturning during the past 150 years. *Nature*, **556(7700)**, 227–230. https://doi.org/10.1038/s41586-018-0007-4

Van Sebille, E., and Coauthors, 2018: Lagrangian Ocean Analysis: Fundamentals and Practices, *Ocean Modelling 121*: 49 - 75. https://doi.org/10.1016/j.ocemod.2017.11.008.

Velicogna, I., and Coauthors, 2020: Continuity of Ice Sheet Mass Loss in Greenland and Antarctica From the GRACE and GRACE Follow-On Missions, *GRL*, **47(8)**, https://doi.org/10.1029/2020GL087291

Yang, Q., and Coauthors, 2016: Recent increases in Arctic freshwater flux affects Labrador Sea convection and Atlantic overturning circulation. *Nature Communications*, **7**, 10525. https://doi.org/10.1038/ ncomms10525

Yashayaev, I., D. Seidov, and E. Demirov, 2015: A new collective view of oceanography of the Arctic and North Atlantic basins. Progress in Oceanography, **132**, 1–21. https://doi.org/10.1016/j.pocean.2014.12.012

Yashayaev, I., and J. W. Loder, 2016: Recurrent replenishment of Labrador Sea Water and associated decadal-scale variability. *Journal of Geophysical Research: Oceans*, **121**, 8095–8114. https://doi.org/10.1002/2016JC012046

Yashayaev, I., and J. W. Loder, 2017: Further intensification of deep convection in the Labrador Sea in 2016. *Geophysical Research Letters*, **44**, 1429–1438. https://doi.org/10.1002/2016GL071668

Zhu, J., and E. Demirov, 2011: On the mechanism of interannual variability of the Irminger Water in the Labrador Sea, *J. Geophys. Res.*, **116**, C03014, doi:10.1029/2009JC005677.

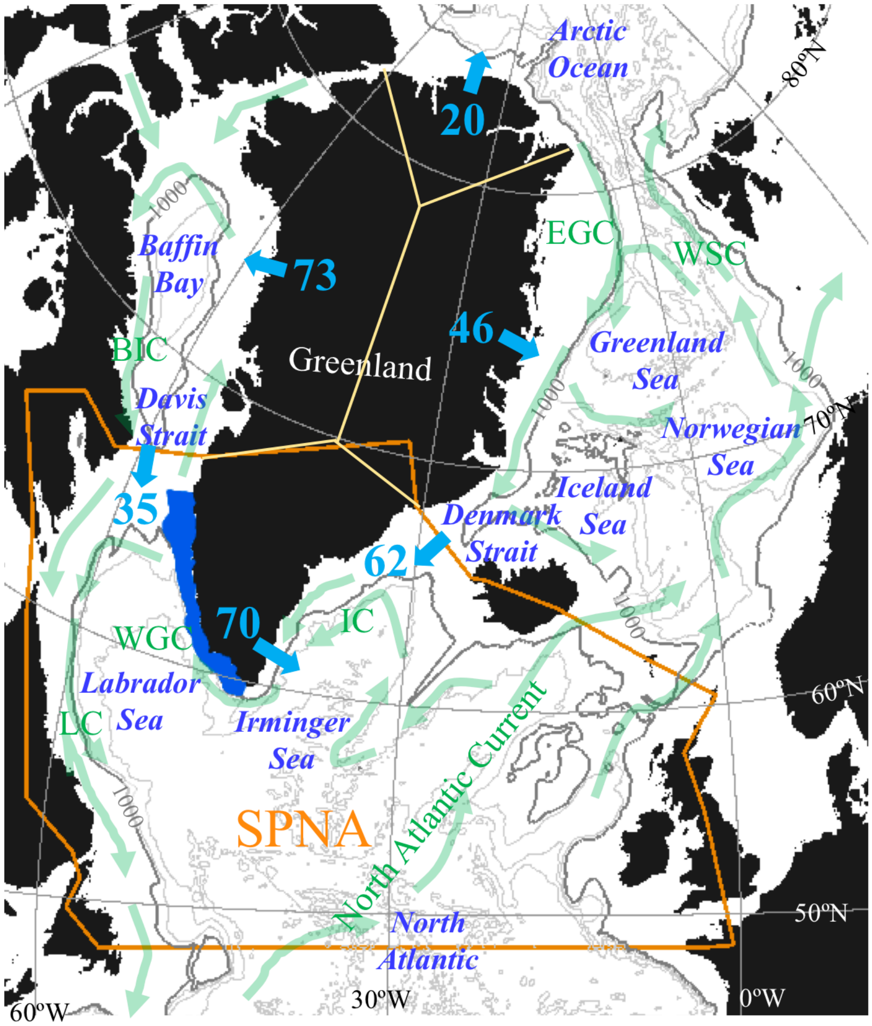


Figure 1. The study domain includes the Subpolar North Atlantic (bounded by the orange contour). The grey contours are isobath drawn every 1000 m, the 1000-m isobath is dark grey. The blue arrows and numbers indicate annual mean surplus Greenland freshwater fluxes and transports through Davis and Denmark Straits (km$^3$ yr$^{-1}$). For Greenland, the mean annual freshwater flux anomalies (deduced from Greenland runoff data of Bamber et al., 2018) are integrated for 4 regions. The oceanic transports of the GFWA through the Davis and Denmark straits are estimated from the HYCOM model experiments with passive tracers tracking GFWA. The dark blue shaded area over the southwestern shelf designates release locations of Lagrangian

particles discussed in section 4.2. The light greenl arrows represent major currents including the North Atlantic Current, Irminger Current (IC), East Greenland Curent (EGC), West Greenland Current (WGC), Labrador Current (LC), West Spitsbergen Current (WSC), Baffin Island Current (BIC).

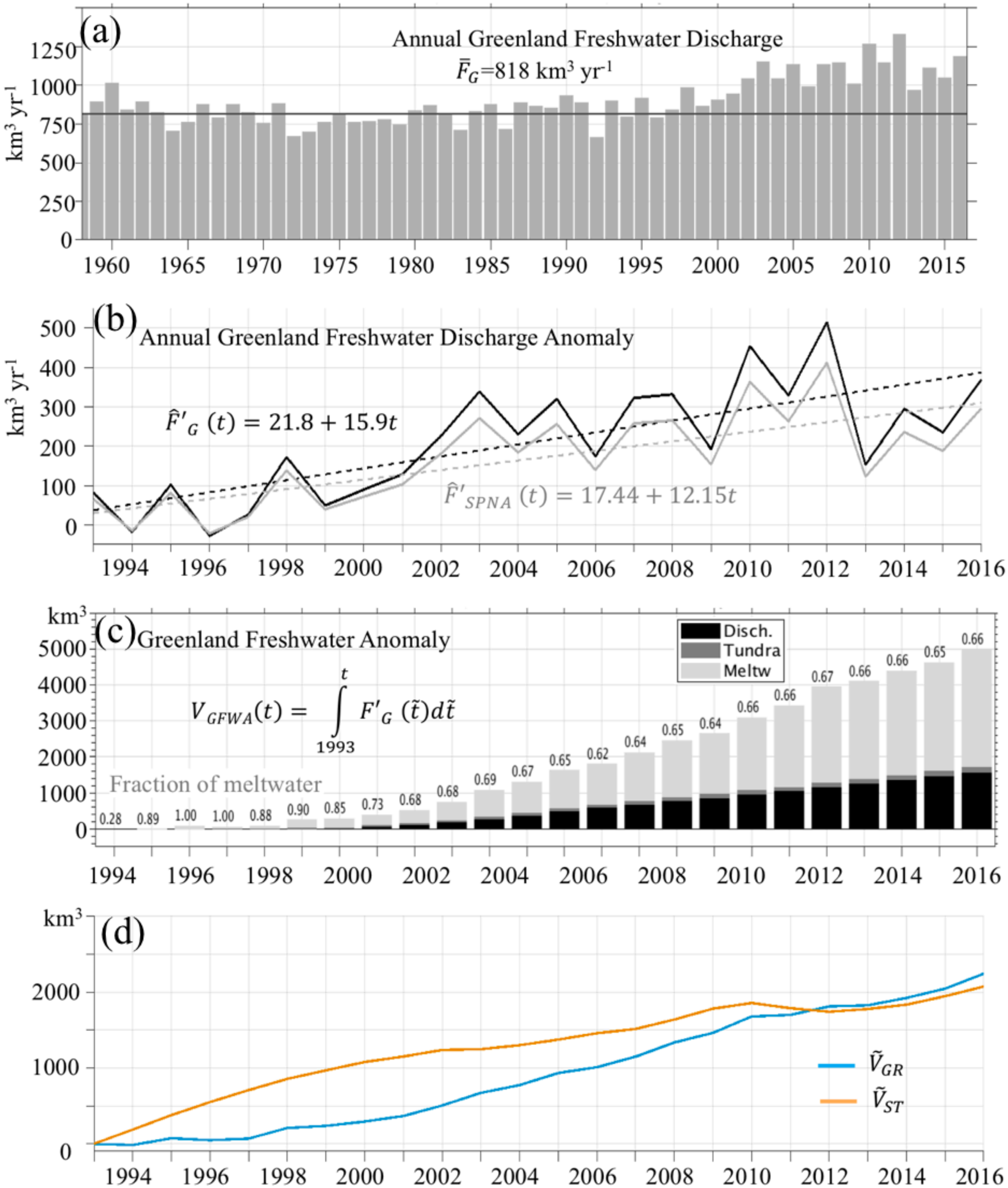


Figure 2. Greenland freshwater mean and anomaly fluxes. (a) Annual total Greenland freshwater discharge (km$^3$ yr$^{-1}$) derived from the monthly gridded product by Bamber et. (2018). The

horizontal solid line is the mean flux over 1958–1993 ($\bar{F}_G$ = 818.3 km$^3$ yr$^{-1}$) used as a reference for calculating the GFWA. (b) Annual Greenland freshwater flux anomaly ($F'_G$). The grey solid curve is the fraction of the Greenland freshwater flux anomaly advected to the SPNA (section 2.3). The dashed lines are linear trends. (c) Time integration of the Greenland freshwater flux anomalies yields GFWA. The digram shows time series of the GFWA and its components. The numbers indicate the fraction of meltwater in the total GFWA. (d) Time series of the volume of the GFWA accumulated in the SPNA estimated from the HYCOM tracer numerical experiments. The blue line is GFWA accumulation for experiment forced with monthly Greenland FW anomaly fluxes shown in (b) ($\tilde{V}_{GR}$). The orange line is GFWA accumulation with the GFWD anomaly kept constant after 1993 ($\tilde{V}_{ST}$).

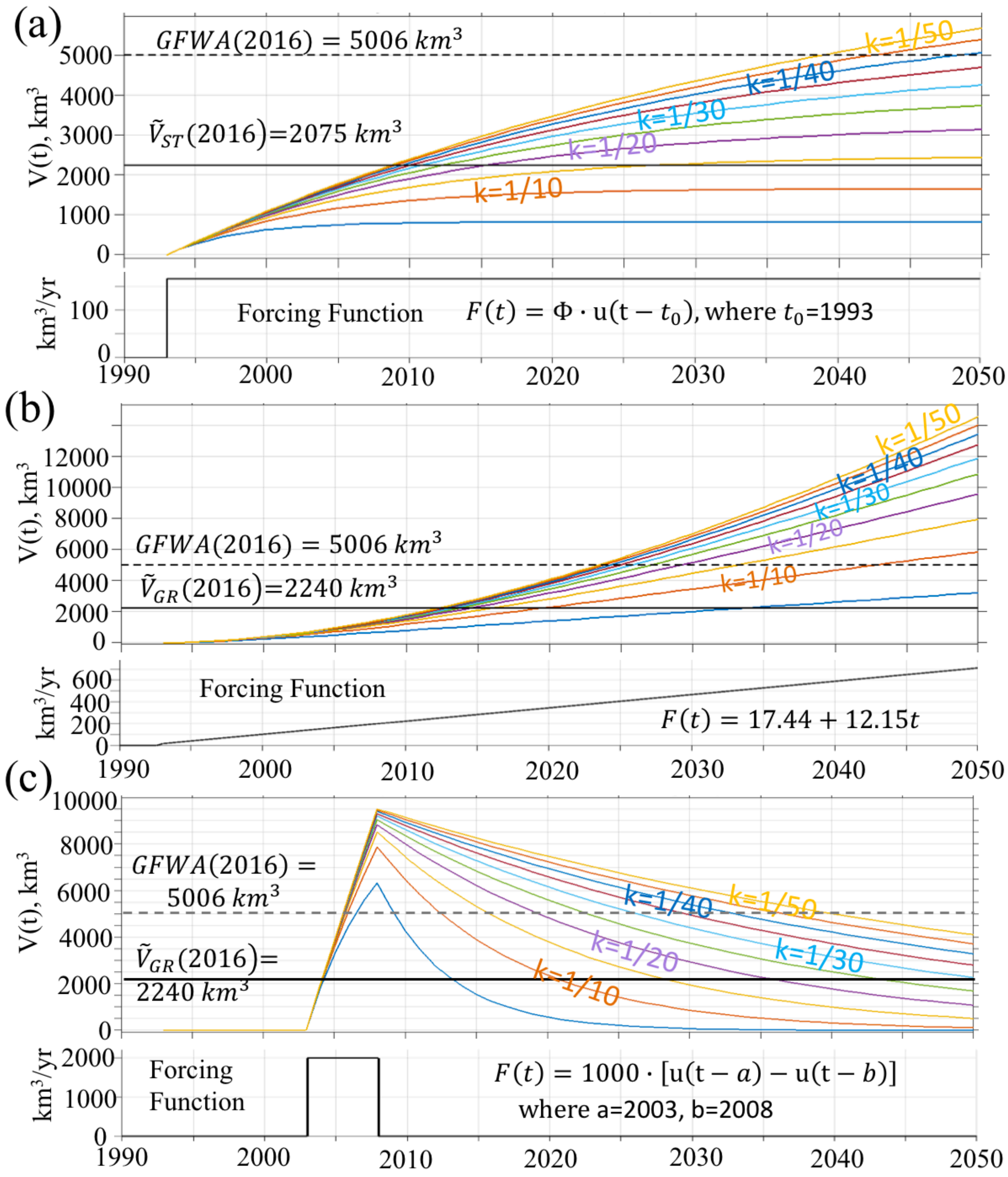


Figure 3. Solutions for equation (4) with $V_0 = 0$ showing progress of GFWA accumulation in the SPNA under different forcing. (a) Solutions with constant ($\Phi$ = 167 km$^3$·yr$^{-1}$) Greenland

freshwater discharge anomaly (equation 8) for different $k$. The forcing imposed as a step function in year 1993 (bottom panel). The dashed line is GFWA by the end of 2016 (5006 km$^3$). The black solid lines is the GFWA accumulated in the SPNA by the end of 2016 estimated from the HYCOM tracer experiments (figure 2d). (b) Same as (a) but for the linearly increasing discharge rate anomaly (equation 2). (c) Same as (a) but for the bump forcing function.

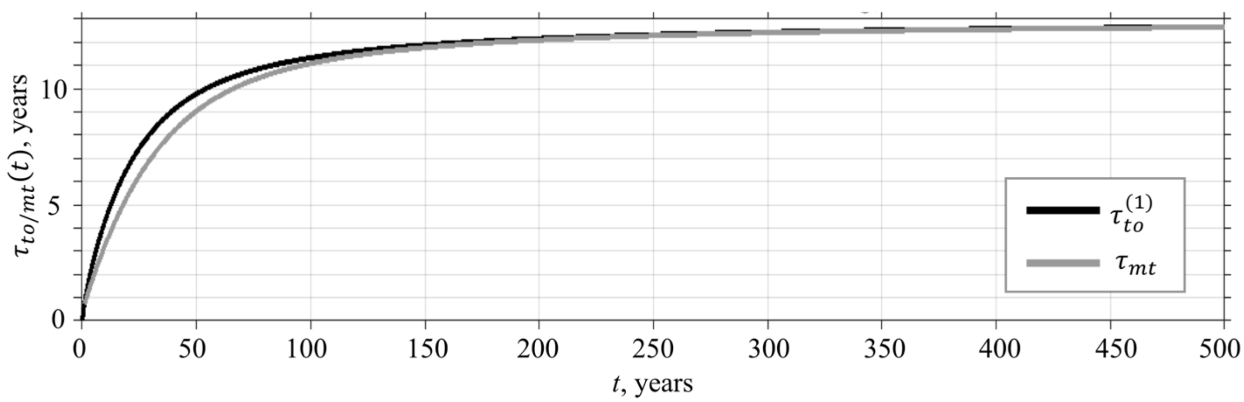


Figure 4. Turn-over time (eq. 13) and mean transit time (eq. 15) of the GFWA for the linearly-increasing flux of the GFWA into the SPNA. The time scales converge to the time scale $\tau = k^{-1} = 13$ years obtained from eq. (4).

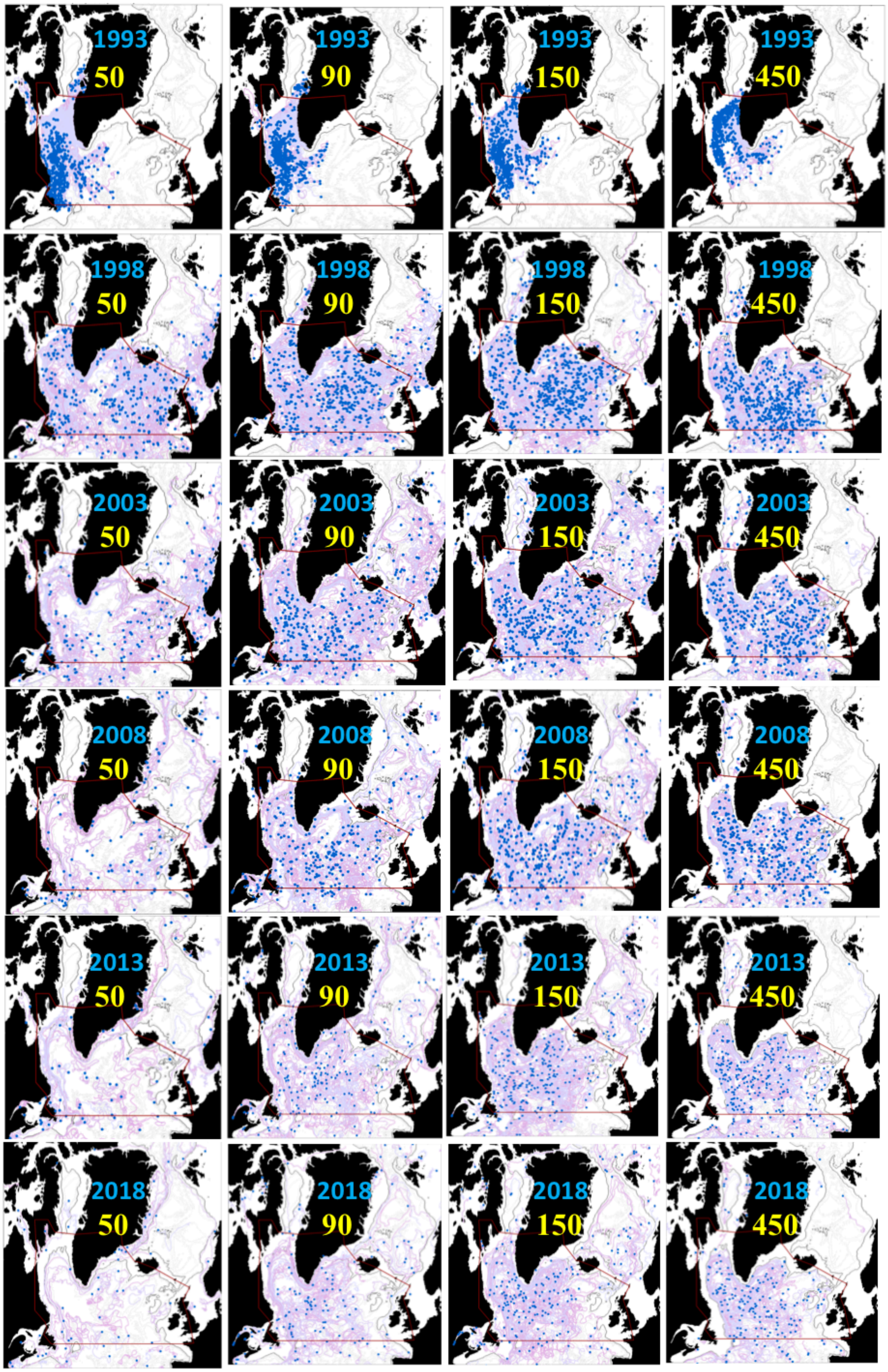
1993
50
1993
90
1993
150
1993
450
1998
50
1998
90
1998
150
1998
450
2003
50
2003
90
2003
150
2003
450
2008
50
2008
90
2008
150
2008
450
2013
50
2013
90
2013
150
2013
450
2018
50
2018
90
2018
150
2018
450

Figure 5. Particles' positions and their pathways at the end of the every 5$^{th}$ year starting 1993. The pathways are shown for the current year. The particles' groups are shown in columns, the years are in rows.

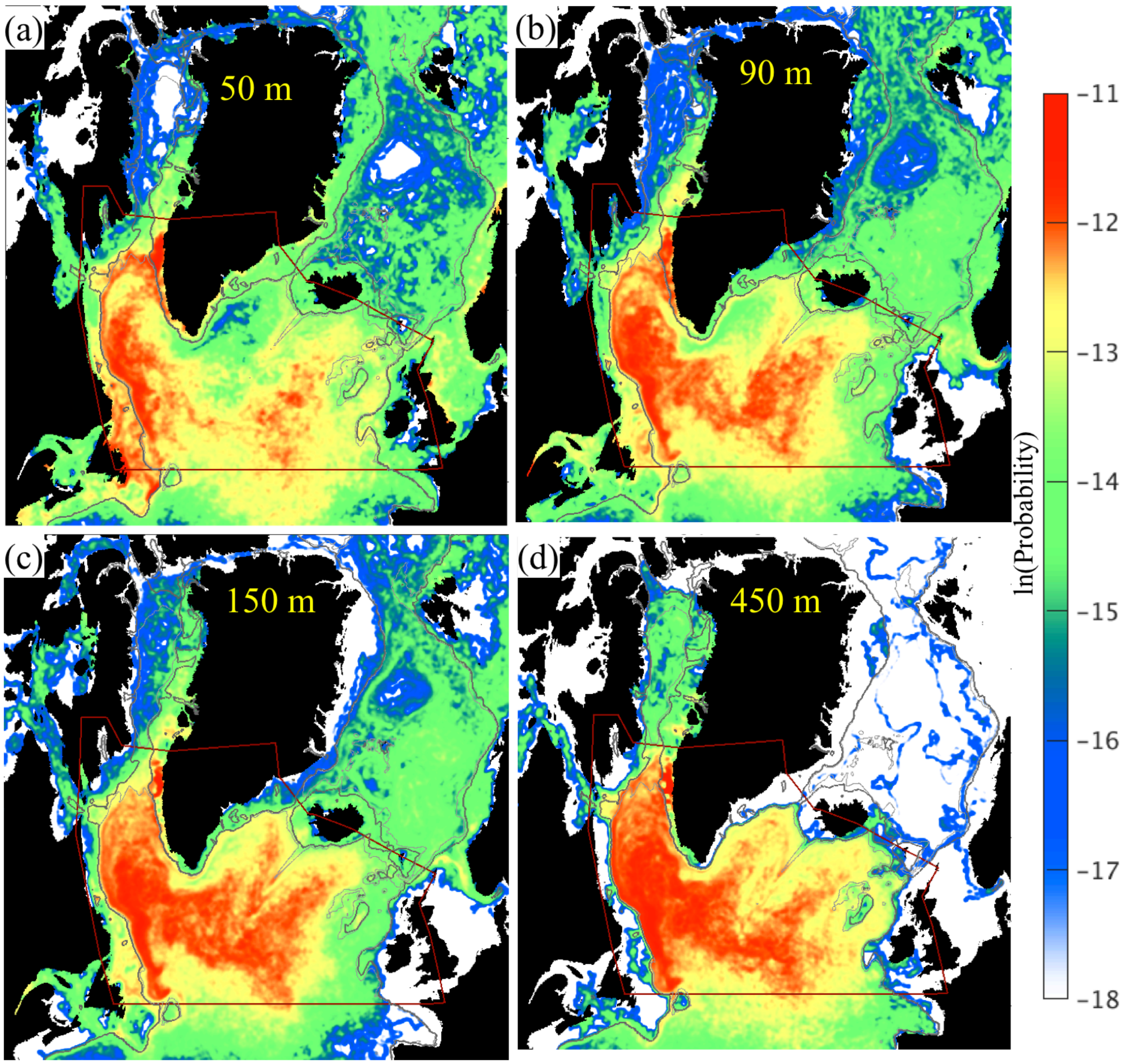

Figure 6. Probability maps of observing a particle in a grid cell at any given day during the time of integration (1993–2019) for particles advected at 50 m (a), 90 m (b), 150 m (c), and 450 m (d). The colors designate the probabilities on a natural logarithmic scale. Integrated across the model domain, the probability is 1. The contour denotes the SPNA region.

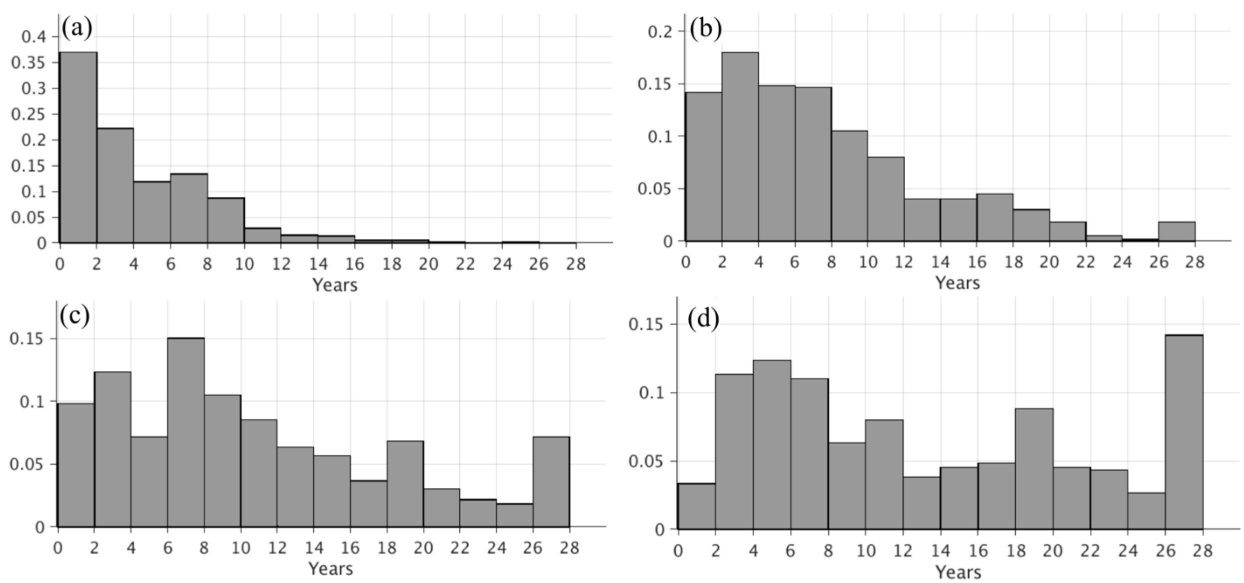


Figure 7. Particle age or transit time distribution for the particle groups advected at 50 m (a), 90 m (b), 150 m (c), and 450 m (d). The vertical axis is frequency. The horizontal axis is particle age or transit time. The inset (e) shows the median (bullets) and the $10^{th}$-$90^{th}$ percentile range of the data for the particle groups labeled with the corresponding nominal depths.

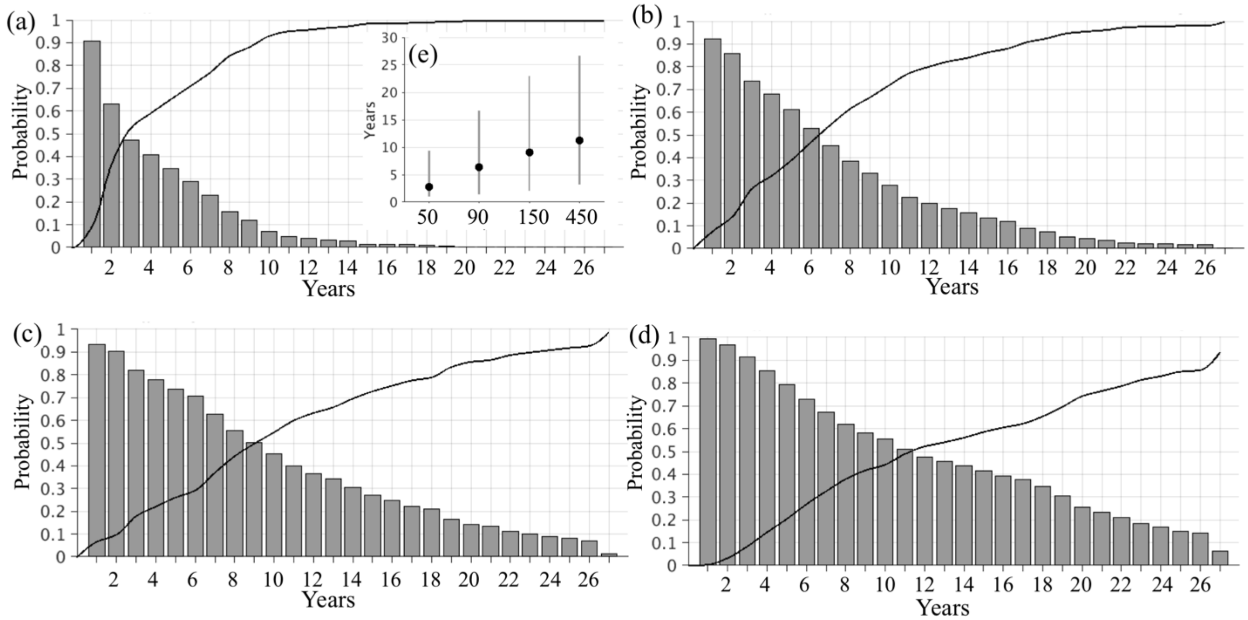


Figure 8. Cumulative probabilities of a particle age and transit time for the particle groups advected at 50 m (a), 90 m (b), 150 m (c), and 450 m (d). The bar diagrams approximate the inverse distribution function showing probability of a particle age or transit time to be at least N years. The lines are the cumulative distribution functions showing the probability that the age or transit time of a particle is at most N years. The inset (e) depicts the median and the interdecile range of particle ages/ transit time in the SPNA for the particle groups labeled with the corresponding nominal depths.

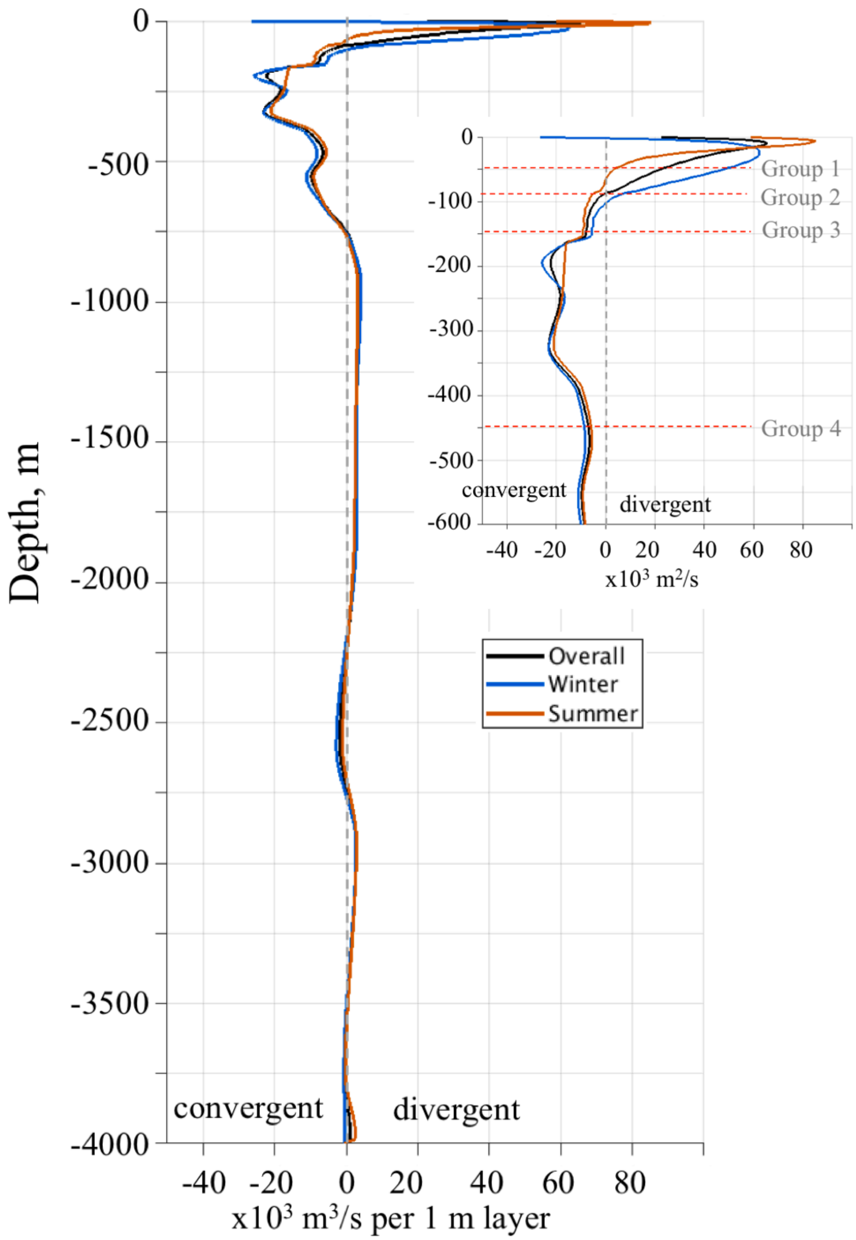


Figure 9. Volume fluxes obtained from the HYCOM experiment and integrated around the SPNA contour (figure 1). The fluxes ($M_i$) are for 1-m thick volumes bounded by $\Gamma_i$ (eq. (17)). The inset is a zoom-in of the upper 600 m. The orange dashed lines indicate approximate depths of the layers where Lagrangian particles were advected.